Tectonophysics 582 (2013) 76–83

Contents lists available at SciVerse ScienceDirect

Tectonophysics

journal homepage: www.elsevier.com/locate/tecto

Rapid long-term erosion in the rain shadow of the Shillong Plateau, Eastern Himalaya

Vikas Adlakha [a], Karl A. Lang [b], R.C. Patel [a], Nand Lal [a], Katharine W. Huntington [b,*]

[a] Department of Geophysics, Kurukshetra University, Kurukshetra-136 119, India
[b] Department of Earth and Space Sciences, University of Washington, Seattle, WA 98122, USA

ARTICLE INFO

Article history:
Received 28 August 2012
Received in revised form 21 September 2012
Accepted 24 September 2012
Available online 3 October 2012

Keywords:
Eastern Himalaya
Low-temperature thermochronology
Exhumation
Erosion
Thermo-kinematic modeling

ABSTRACT

Geodynamic models of collisional orogens suggest that precipitation gradients profoundly influence spatial patterns of exhumation and deformation in active collisional mountain ranges. A basic tenet of this hypothesis is that in unglaciated areas, spatial patterns of long-term precipitation, erosion and exhumation should be correlated. A correlation of this type has been observed in the Eastern Himalaya, where uplift of the Shillong Plateau by Pliocene time drastically reduced monsoonal rainfall in the Himalayan range downwind. Existing apatite fission-track data suggest that the resulting precipitation gradient caused a twofold gradient in long-term erosion rates across an area with similar geology, suggesting a strong influence of climate on the region's geomorphic and tectonic evolution. We extend this dataset by presenting 53 new bedrock apatite and zircon fission-track ages from deeper within the rain shadow. We expected latest Miocene to Pliocene apatite ages, similar to previously published ages from neighboring areas in the rain shadow. Instead, apatites as young as 1.3 ± 0.2 Ma and zircons as young as 4.5 ± 1.0 Ma (2σ) demonstrate that spatial gradients in precipitation do not correlate with variations in long-term erosion and crustal strain as predicted by geodynamic models. Thermal–kinematic modeling of these data suggests that local exhumation patterns reflect gradients in rock uplift dictated by fault kinematics in this rapidly deforming area, despite a dramatic precipitation gradient. These findings both highlight the need to better understand how erosive processes scale with precipitation amount and intensity in such settings, and suggest a disconnect between the predictions of orogen-scale geodynamic models and the relationship between erosion and tectonics at the regional scale.

1. Introduction

The hypothesis that atmospheric and geodynamic processes are strongly coupled through the action of erosion is one of the most exciting geoscience developments of the past few decades. But while most researchers agree that erosion can localize strain and deformation in the crust (e.g., Beaumont et al., 2001; Champagnac et al., 2008; Dahlen and Suppe, 1988; Hilley and Coutand, 2010; Koons et al., 2003; Willett et al., 1993), the influence of climatic gradients on long-term erosion and deformation is less clear. Although the rate of tectonic convergence controls long-term mass fluxes at the orogen scale (Koppes and Montgomery, 2009; Roe and Brandon, 2011), at sub-orogen scales models predict a strong influence of precipitation on erosion and exhumation-related deformation (e.g., Beaumont et al., 1992, 2001; Dahlen and Suppe, 1988; Koons, 1989; Koons et al., 2002; Willett, 1999). Indeed, many field studies have compared exhumation patterns measured over million-year timescales across climatic gradients as characterized by modern precipitation patterns to argue for coupling of climate, erosion and deformation (e.g., Hodges et al., 2004; Patel et al., 2011; Reiners et al., 2003; Thiede et al., 2005). However, the influence of precipitation gradients on long-term erosion is debated (e.g., Burbank et al., 2003), and clear field evidence for a strong coupling of climate, erosion, and deformation on the scale of mountain ranges has proved difficult to find (e.g., Thiede et al., 2009; Vernon et al., 2009; Whipple, 2009).

One place where a coupling of precipitation gradients and long-term erosion has been proposed is the Bhutan Himalaya, where the Shillong Plateau, a 1600-m high orographic barrier in northeast India, drastically reduces precipitation in the Himalayan range downwind (Biswas et al., 2007; Grujic et al., 2006). In this region, the pattern of erosion rates inferred from apatite fission-track (FT) cooling ages mimics the steep gradient in rainfall caused by the Shillong Plateau, leading Grujic et al. (2006) to suggest a climatic control on erosion and rock exhumation over million-year timescales. New constraints on the region's tectonic and structural evolution (Banerjee et al., 2008; Biswas et al., 2007; Clark and Bilham, 2008; McQuarrie et al., 2008; Tobgay et al., 2012; Yin et al., 2010) make it an ideal setting to examine such patterns in the context of deformation.

We build on previous work by presenting 53 new apatite and zircon FT data from a densely sampled transect deeper in the rain shadow in India (Fig. 1) and examining them in the context of recent

* Corresponding author. Tel.: +1 206 543 1750; fax: +1 206 543 0489.
E-mail addresses: vikas.himg@gmail.com (V. Adlakha), karllang@uw.edu (K.A. Lang), patelramesh_chandra@rediffmail.com (R.C. Patel), lalkuk@gmail.com (N. Lal), kate1@uw.edu (K.W. Huntington).

0040-1951/$ – see front matter
http://dx.doi.org/10.1016/j.tecto.2012.09.022

higher-temperature thermochronometer data, structural mapping, and geochronologic constraints on faulting. While our new apatite FT data are directly comparable to the data of Grujic et al. (2006) from the same litho-tectonic units to the west, zircon FT data reflecting a higher closure temperature are more sensitive than young valley bottom apatite samples to differences in erosion rate over million-year timescales, and combined with previous muscovite $^{40}Ar/^{39}Ar$ data (Yin et al., 2010) extend the cooling history of the study area to the Miocene.

2. Tectonic setting and precipitation gradients in the Eastern Himalaya

In the Eastern Himalaya of Bhutan and Arunachal Pradesh, India, continental convergence between India and Eurasia has been accommodated along a series of major north-dipping structures that can be traced along the 2500-km-long Himalayan arc (Fig. 1a) (Gansser, 1983; Hodges, 2000; LeFort, 1975; Yin, 2006). Moving southward from the Tibetan Plateau, the South Tibetan Detachment separates Tethyan Himalayan strata from the underlying Greater Himalayan Sequence (GHS), and the Main Central Thrust (MCT) places the GHS above the Lesser Himalayan Sequence (LHS). Similar to some other parts of the range, in the Eastern Himalaya the MCT forms the roof of a duplex (Long et al., 2011; McQuarrie et al., 2008; Tobgay et al., 2012; Yin et al., 2006, 2010), and several major thrust faults have been mapped in its footwall in Arunachal (Yin et al., 2010). Although Quaternary deformation and active thrust faulting at the position of the MCT are indicated by observations from some parts of the Central Himalaya (e.g., Hodges et al., 2004; Huntington and Hodges, 2006; Huntington et al., 2006; Wobus et al., 2003, 2005), the MCT in Arunachal has been folded and is cut by east-dipping normal faults of the Cona Rift zone, indicating that it is no longer active (Yin et al., 2010). In the footwall of the MCT, the LHS is bounded below by the Main Boundary Thrust, and the underlying sub-Himalayan strata are deformed by the Main Frontal Thrust zone. These thrusts are thought to sole into a mid-crustal décollement at depth, the Main Himalayan Thrust (MHT; Jackson and Bilham, 1994).

Although this sequence suggests along-strike uniformity, the structure, tectonics and geomorphology of the Eastern Himalaya are unique in several respects (e.g., Bookhagen and Burbank, 2006, 2010; Yin, 2006). One key difference is that in the east the Shillong Plateau, a 400-km-long anticlinal basement fold (Clark and Bilham, 2008; Das Gupta and Biswas, 2000) or pop-up structure (Biswas et al., 2007) rises ~1600-m from the Gangetic Plain between ~90 and 93°E, creating the only topographic barrier in the Himalayan foreland for moisture sourced from the Bay of Bengal.

The Shillong Plateau strongly influences rainfall across the Eastern Himalaya, reducing mean annual precipitation in the rain shadow to half of that observed in neighboring regions (Biswas et al., 2007; Bookhagen and Burbank, 2010; Grujic et al., 2006; Fig. 1b). The east–west gradient is even more pronounced during the Indian summer monsoon, which accounts for 90% of precipitation in the region (Bookhagen and Burbank, 2010) and was established by the late Miocene (ca. 12–8 Ma; e.g., An et al., 2001; Dettman et al., 2001, 2003; Molnar et al., 1993), or possibly much earlier (e.g., Clift et al., 2008; Guo et al., 2002; Sun and Wang, 2005). Although past intensified monsoon phases might have delivered more precipitation deeper into higher elevation regions (Bookhagen et al., 2005a,b), as long as the orography remained unchanged, variations in monsoon strength would not change the location of the major peak in rainfall at the Himalayan range front or the strong east–west precipitation gradient (Bookhagen and Burbank, 2010; Grujic et al., 2006). Recent thermochronometric studies show that deformation of the Shillong Plateau began by 8–14 Ma, with rock uplift rates outpacing erosion by a factor of two or more (Clark and Bilham, 2008), and suggest the establishment of the orographic barrier and general east–west precipitation gradient at least by Pliocene time (Biswas et al., 2007).

3. Low-temperature thermochronology

In the Bhutan Himalaya, previous apatite FT data suggest a correlation between the pattern of long-term erosion rates and steep rainfall gradients that have persisted for millions of years in the wake of the Shillong Plateau (Grujic et al., 2006; Fig. 1). Apatite FT ages record the time since cooling from ~90 to 120 °C and are commonly interpreted to reflect relative 10^6-yr averaged erosion rates (e.g., Braun et al., 2006; Ketcham et al., 2007). In western Bhutan, in the zone of intense monsoonal precipitation outside the rain shadow of the Shillong Plateau, apatite FT ages as young as 1.4 Ma indicate rapid erosion at 1.0–1.8 mm/yr (Grujic et al., 2006). In eastern Bhutan, within the rain shadow, older ages (most ~6 Ma) suggest a twofold decrease in erosion rates, leading previous workers to argue for a spatial correlation and causal link between precipitation and long-term erosion (Biswas et al., 2007; Grujic et al., 2006).

We estimate long-term erosion rates deeper in the rain shadow by dating bedrock samples along a 100-km transect in Arunachal using both apatite and zircon FT thermochronometry (Figs. 1b and 2; see Appendix A for details of methods and results). Zircon FT data reflect cooling through ca. 230–330 °C (Tagami and Shimada, 1996) and extend cooling history constraints to Miocene time. The densely sampled transect crosses all major structures in both the GHS and LHS, including the Bomdila Thrust in the footwall of the MCT (Yin et al., 2010). Consequently, we can also use the spatial pattern of thermochronometer ages to examine the degree to which cooling might reflect not only regional precipitation gradients but also local fault kinematics.

Following the hypothesis of Grujic et al. (2006), we would expect our new analyses from Arunachal to reveal ages similar to those observed in the rain shadow in eastern Bhutan with all else being equal. Systematic changes in convergence rate (Banerjee et al., 2008; Styron et al., 2011) and river steepness patterns across the study area (Fig. A1) are not observed. Nevertheless, along-strike structural variability (e.g., Tobgay et al., 2012; Yin et al., 2010) may contribute to variations in fracture density, influencing erodibility (Molnar et al., 2007). However, some of the new GHS samples from Arunachal were collected at similar structural levels and within only ~25 km of samples analyzed by Grujic et al. (2006) (Figs. 1b, 2), and although fracture density may vary across this zone, there is no reason to expect a priori that the strength of GHS rocks of similar lithology should change systematically from east to west. Thus if precipitation is the main driver of long-term erosion and exhumation, the new apatite FT ages should fit the previously observed correlation of ages with the east–west precipitation gradient.

We expected cooling ages similar to those in nearby eastern Bhutan (~6 Ma), but instead we find cooling ages in the GHS of Arunachal just as young as the youngest ages observed by Grujic et al. (2006) in rapidly eroding western Bhutan (Table A1). Apatites as young as 1.3 ± 0.2 Ma (2σ) suggest similarly high Pleistocene erosion rates of 1.0–1.8 mm/yr (Grujic et al., 2006), and zircons as young as 4.5 ± 1.0 Ma (2σ) indicate that rapid cooling and exhumation extended to the Pliocene (Table A1). Together with published muscovite $^{40}Ar/^{39}Ar$ ages from the GHS (Yin et al., 2010) reflecting cooling through ca. 425 °C (Harrison et al., 2009), the data indicate rapid average cooling rates of 40 °C/Myr since at least 12 Ma in the hanging wall of the MCT (Fig. 3a).

In contrast, both apatite and zircon FT ages for LHS rocks along our transect are much older (5.7–9.7 Ma and 10.9–14.1 Ma, respectively), reflecting slower cooling. Although the average (linear) cooling rate of the LHS since 14 Ma is 20 °C/Myr—half that of the GHS over this interval, the apatite FT data require an even lower average LHS cooling rate of just 13 °C/Myr post ~9 Ma (Fig. 3a). Time–temperature paths constrained by the thermochronometer data show that temperatures for GHS and LHS rocks along our transect now juxtaposed at the

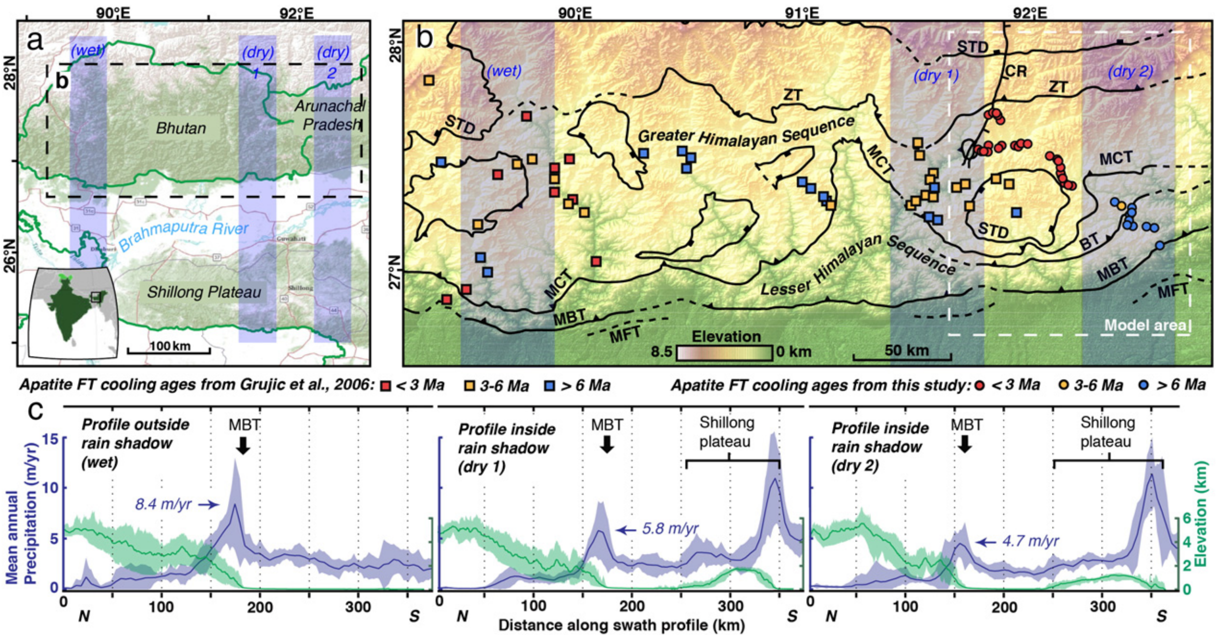

Fig. 1. Tectonic setting, sample locations, and precipitation patterns in the Eastern Himalaya. (a) Overview map indicates country borders (green lines) and map area in (b) (dashed rectangle). Shaded blue swaths (wet, dry 1, dry 2) correspond to the precipitation and elevation profiles shown in (c). (b) Apatite FT data (circles) from this study and from Grujic et al. (2006), with faults after Grujic et al. (2002) and Yin et al. (2010) (black lines, dashed where inferred): STD, South Tibetan Detachment; CR, Cona Rift; ZT, Zimithang/Khangtang Thrust; MCT, Main Central Thrust; BT, Bomdila Thrust; MFT, Main Frontal Thrust. GHS and LHS are Greater Himalayan Sequence and Lesser Himalayan Sequence, respectively. Dashed white rectangle shows model area in Fig. 4a. (c) Precipitation and elevation profiles corresponding to swaths shown in (a). Precipitation data were sourced from the Tropical Rainfall Monitoring Mission (TRMM) and post-processed, with values calculated from 1998 to 2006 mean annual precipitation (m/yr) at 5 × 5 km resolution (Bookhagen and Burbank, 2006, 2010). Blue lines are mean annual precipitation rate, and shaded regions show 2σ variation across swaths. Elevation data are from the World Wildlife Federation HydroSHEDS dataset, sourced from the Shuttle Radar Topographic Mission (SRTM) and processed to fill holes and abnormalities. The horizontal resolution is ~90 m and the vertical resolution is 16 m. Green lines are mean elevation, and shading indicates 2σ variation across swaths.

surface differed by at least 50 °C and probably > 100 °C at 2.5 Ma (Fig. 3b).

In summary, our most important finding is that in the rain shadow in Arunachal, FT cooling ages for apatites from the GHS are uniformly young (average 2.1 Ma, standard deviation 0.4 Ma, n = 28), indicating erosion rates that are just as rapid as rates estimated for an area with much higher peak mean annual rainfall in western Bhutan (Grujic et al., 2006). Combined with zircon FT ages for the GHS (n = 7) and apatite and zircon FT ages from the LHS (n = 18), the data reveal an abrupt offset in cooling ages and rates along our transect. In the following sections we discuss possible reasons for this offset and for the lack of correlation between long-term erosion rates and modern precipitation.

4. Local cooling-age patterns and thermal–kinematic modeling

The striking offset in cooling ages and rates across a short distance (<12 km) suggests that the local pattern of exhumation and long-term erosion in this area is a response to differential rock uplift related to faulting. We explore this possibility by modeling thermochronometer ages as a function of varying fault kinematics. Our goal is not to invert the data for a unique solution, but rather to demonstrate whether or not kinematic scenarios consistent with geologic constraints in the region can easily explain the pattern of ages observed along the transect.

Thermochronometer ages vary as a function of the paths and rates at which rocks are exhumed through the subsurface thermal field. We forward modeled the subsurface thermal field resulting from heat production, conduction, and advection along faults, and predicted cooling ages along the sample transect using a modified version of the three-dimensional finite-element code Pecube (Braun, 2003). Motion along modeled faults is entirely dip-slip, with no accompanying shear heating. Faults are not advected in the model, and particles move parallel to fault segments. Thermal parameters were homogenous throughout the modeled volume and consistent with values estimated from previous models of the eastern and central Himalaya (Herman et al., 2010; Robert et al., 2009, 2011) (see Appendix A, Tables A2–4). The models assume a steady-state topography, since evolving topography had a minor influence on the output of similar models of the central Himalaya (Herman et al., 2010). Models were run for 13 or 18 Myr durations, and cooling ages were calculated using forward diffusion and annealing models for the $^{40}Ar/^{39}Ar$ and FT systems (Braun et al., 2006). The misfit between the predicted and observed thermochronometer ages from this study was assessed using the root-mean-square (RMS) misfit, in millions of years, for each thermochronometer and for the dataset as a whole.

Model realizations (n = 560) were carried out to explore the effects of fault geometry and kinematics on predicted cooling ages (Fig. 4a; see Appendix A, Tables A2–4 for model parameters). Cooling was driven by exhumation either along a crustal scale ramp (Main Himalayan Thrust–Main Frontal Thrust) or partitioned between the ramp and an out-of-sequence reverse fault, similar to previous models west of the sampled area (e.g., Herman et al., 2010; Robert et al., 2009, 2011). The flat-ramp structure of the MHT is based on published maps and cross-sections (Yin et al., 2010). The modeled reverse fault extends from the bottom of the ramp to the surface where cooling ages are offset at the GHS–LHS contact. For all models, India–Asia plate convergence was held constant at 21 km/Myr and partitioned between overthrusting (V_o) and underthrusting (V_u) (see discussion in Robert et al., 2011). For the ramp models, V_o/V_u was varied for a range of MHT fault dips (see Appendix A). For models invoking the out-of-sequence reverse fault, V_o was partitioned into the ramp velocity component (V_r) and the reverse fault velocity component (V_f), such that V_r and V_f sum to V_o. A final suite of models delayed the activation of the out-of-sequence reverse fault until time t (where $0.5 \leq t \leq 9$ Ma), at which point V_o was partitioned onto V_r

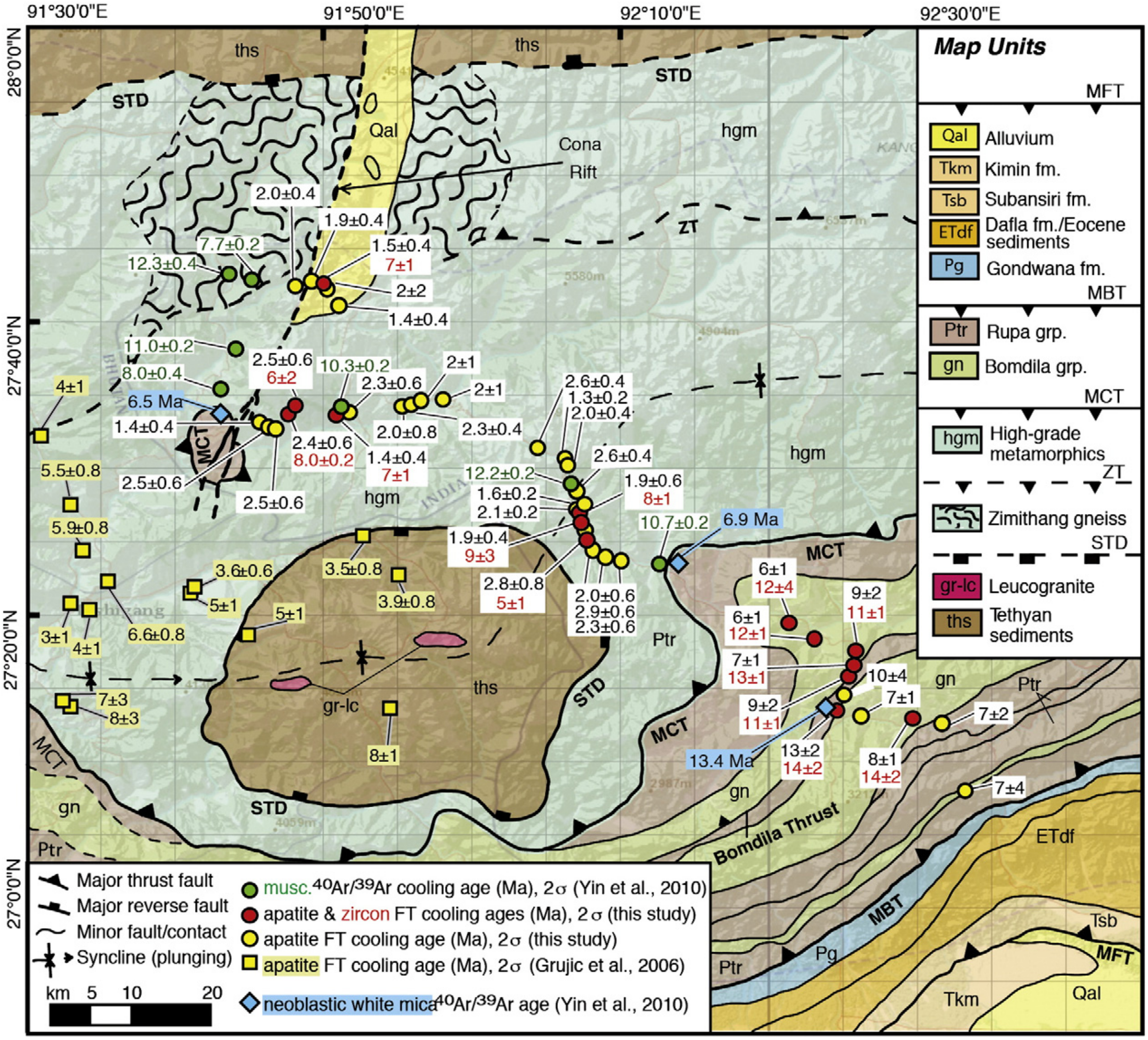

Fig. 2. Thermochronometer data with bedrock geology after Yin et al. (2010). Major structures include the Main Frontal Thrust (MFT), Main Boundary Thrust (MBT), Main Central Thrust (MCT), Bomdila Thrust, Khangtang (or Zimithang) Thrust (ZT), South Tibetan Detachment (STD), and Cona Rift. Yellow circles are apatite FT samples from this study, and red circles are samples from this study with both apatite and zircon FT data. Yellow squares are apatite FT data of Grujic et al. (2006). Green circles are muscovite $^{40}Ar/^{39}Ar$ cooling ages from Yin et al. (2010). Blue diamonds are $^{40}Ar/^{39}Ar$ ages for white mica associated with cleavage development near the MCT, interpreted to represent crystallization of new (neoblastic) mica crystals (e.g., Dunlap et al., 1997) and constrain fault timing (Yin et al., 2010). Note: in the SW part of the map, there is some discrepancy between the locations of structures on the maps of Grujic et al. (2006) and Yin et al. (2010); sample locations from previous studies are plotted using published coordinates.

and V_t. These delayed fault onset models used the best-fit geometric and kinematic parameters from the crustal ramp and reverse fault models.

While a wide range of models can explain both our apatite FT ages and the previously published ages of Grujic et al. (2006) within the model area, the simplest kinematic scenarios we explored cannot explain the higher-temperature thermochronometer data (Fig. 4b); this is because while low-closure temperature valley bottom apatite samples are relatively insensitive to differences in exhumation rate and pathway, the spatially limited zircon and muscovite data more effectively discriminate among model scenarios. In the simplest scenario, all shortening is accommodated on the MHT, and GHS cooling is driven by exhumation above the crustal-scale ramp. These "ramp" models slightly over-predict our apatite FT ages and systematically under-predict both the zircon FT and muscovite $^{40}Ar/^{39}Ar$ cooling ages at the base of the GHS (RMS misfit of preferred model = 2.02 Myr; Fig. 4b, Table A4). Including the out-of-sequence reverse fault increases differential cooling between the GHS and LHS and more accurately predicts all cooling ages (RMS misfit = 1.72 Myr; Fig. 4c), with most of the improvement resulting from increasing zircon FT ages in the LHS. "Reverse fault" models with a wide range of fault geometries predict the FT ages more accurately than the best "ramp" model. However, neither model scenario can explain the muscovite $^{40}Ar/^{39}Ar$ ages in the GHS.

To explain these data, we use the preferred reverse fault model geometry and simulated a two-step kinematic scenario in which the onset of reverse faulting is delayed (Fig. 4c). Such a scenario is suggested by $^{40}Ar/^{39}Ar$ ages for neoblastic white mica associated with cleavage development near the MCT, which are thought to reflect 6–7 Ma out-of-sequence activation of the Bomdila Thrust following the onset of thrust motion at structurally lower levels at ca. 13 Ma (Yin et al., 2010; Fig. 2). Models in which modest out-of-sequence faulting initiates between 6.5 and 8.5 Ma provide a better fit to the cooling-age data (RMS misfit = 1.46 Myr) than the constant

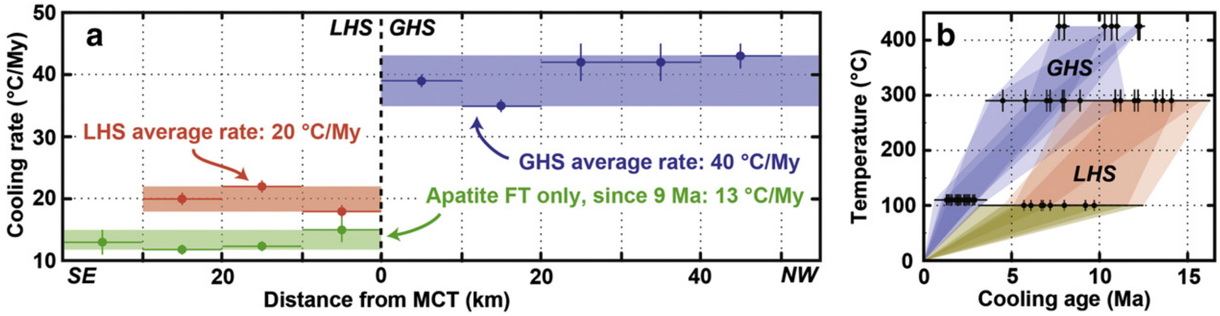

Fig. 3. Cooling rate estimates based on data for multiple thermochronometers. (a) Cooling rate vs. distance along the sample transect; cooling rate was calculated for all available FT and $^{40}Ar/^{39}Ar$ data for each 10-km bin using a least squares linear regression of cooling age and nominal closure temperature (T_C). Nominal closure temperatures consistent with mineral-isotopic system and cooling rate (with nominal 2σ uncertainties) are taken to be 110 ± 20 °C for the FT system in GHS apatites and 100 ± 20 °C for more slowly cooled LHS apatites (Ketcham et al., 2007); 290 ± 40 °C, in the mid range for zircon FT (Foster et al., 1993; Tagami and Shimada, 1996); and 425 ± 50 °C for muscovite $^{40}Ar/^{39}Ar$ (Harrison et al., 2009). Surface temperature in the regressions is 10 ± 10 °C (2σ). Circles indicate the cooling rate for each 10-km bin, and vertical lines indicate 1σ uncertainty in the slope of the regression. Red and blue circles indicate rates calculated using all available thermochronometer data for the LHS (average: 20 ± 2 °C/Myr) and GHS (average: 40 ± 3 °C/Myr), respectively. Green circles indicate LHS rates averaged over a shorter time period, calculated using only apatite FT data and surface temperature. (b) Black circles are cooling age vs. nominal closure temperature for all individual samples with 2σ uncertainties. Each shaded polygon outlines the data (including 2σ age uncertainty) for one 10-km bin, highlighting the difference between the cooling paths for the GHS (blue) and LHS (red).

slip-rate models, particularly improving muscovite $^{40}Ar/^{39}Ar$ age predictions (Fig. 4c).

The key observation is that kinematic scenarios including ongoing displacement on the Main Frontal Thrust and late-Miocene out-of-sequence reverse faulting easily capture both the observed jump in FT ages across the GHS–LHS contact and the pattern of mid-Miocene $^{40}Ar/^{39}Ar$ cooling ages along our transect. Additional apatite FT data are available to the west of our model area (Grujic et al., 2006), but since those ages do not necessarily correlate with mapped surface structures and the apatite FT system is relatively insensitive to the different model scenarios, these data do not allow us to extend the modeling exercise to the west. Nevertheless, for the model area, the fact that a simple, geologically reasonable scenario can explain thermochronometer data sensitive to a wide range of closure temperatures in both the GHS and LHS suggests that fault-controlled variations in rock uplift may control the pattern of long-term erosion and exhumation.

5. Regional cooling-age patterns

Although the model results are non-unique, structural control provides a simple explanation for the cooling-age pattern in our densely sampled transect, and it may also help explain along-strike variations in cooling ages across the region (Fig. 1). While apatite FT ages for some nearby samples analyzed in this study and in Grujic et al. (2006) agree within error, apatites are generally older to the west and south of our transect, where ages for GHS samples within ~15 km of each other vary from 3 ± 1 to 8 ± 3 Ma (2σ) (Fig. 2; samples BH64, BH90, BH53, BH52 of Grujic et al., 2006); there is some discrepancy between the precise positions of structures mapped by Grujic et al. (2006) and Yin et al. (2010) in this area, but neither map shows a fault offsetting these samples. Although east-dipping normal faults of the Cona Rift zone extend from southeastern Tibet to the Himalaya in this area (Fig. 2; Armijo et al., 1986; Taylor et al., 2003; Yin, 2000; Yin et al., 2010), limited muscovite and apatite cooling data across the southern part of the rift zone do not show significant age variation, suggesting that this structure cannot explain the observed apatite FT age variations (Yin et al., 2010). Nevertheless, large-scale folds have been mapped in the area, and perhaps differential motion across unmapped structures or along-strike variations in the position or dip of a subsurface ramp contributes to cooling age variations here. While it is possible that some local and regional variations in apatite FT ages may reflect differences between relict and incised portions of the landscape (Grujic et al., 2006), differential motion across unidentified structures cannot be ruled out without more detailed mapping across the eastern Bhutan–Arunachal border region.

Whatever the precise role of fault kinematics in controlling the observed cooling age patterns is, our key finding is that precipitation and long-term erosion in the Eastern Himalaya are not spatially correlated. In the central Nepal Himalaya, Burbank et al. (2003) argued that the lack of correlation between apatite FT ages and a strike-perpendicular precipitation gradient could be explained by the efficiency of glacial erosion in the higher-elevation portions of the landscape, a hypothesis supported by modern erosion rate patterns (Gabet et al., 2008). But if past glaciation was a factor, it is unclear how it could explain the pattern of younger cooling ages in the drier, currently slightly lower-elevation region in the rain shadow in Arunachal (Fig. 1c). Even if elevation along the Eastern Himalaya decreased since ~10 Ma (Iaffaldano et al., 2011), such regional changes would have impacted glaciation across the entire study area, likely leading to slower erosion and exhumation through time, not rapid erosion and exhumation in the rain shadow over the last few million years. We must conclude that more precipitation does not simply equal more erosion across areas of similar geology here.

A possible explanation for this finding is that increased mean annual and monsoonal precipitation does not cause a corresponding increase in erosional efficiency in this setting, perhaps because erosion is insensitive to changes in precipitation above some threshold or because discharge varies independently of precipitation rate (e.g., Lague et al., 2005; Molnar, 2001; Tucker and Bras, 2000; Tucker and Slingerland, 1997). For example, because high-intensity storms are triggered in the lee of orographic barriers, rainfall intensity varies little along strike despite strong differences in mean annual rainfall (Bookhagen and Burbank, 2010); we might not expect the erosional efficiency of such storms to match the two-fold east–west precipitation gradient across the rain shadow if hillslopes are near a threshold angle for failure (Burbank et al., 1996) or erosion and mass wasting are moderated by the effects of dense vegetation. Indeed, recent models and data for bedrock rivers suggest that erosion rates may be insensitive to increases in runoff exceeding a certain threshold discharge, and that climatic influence on long-term erosion and tectonics in unglaciated landscapes may be restricted to sub-humid or drier climates (DiBiase and Whipple, 2011).

Under such circumstances, efficient erosion would remain focused in the GHS throughout the region once the orography and monsoon were established and–if there is a strong climate–erosion–exhumation

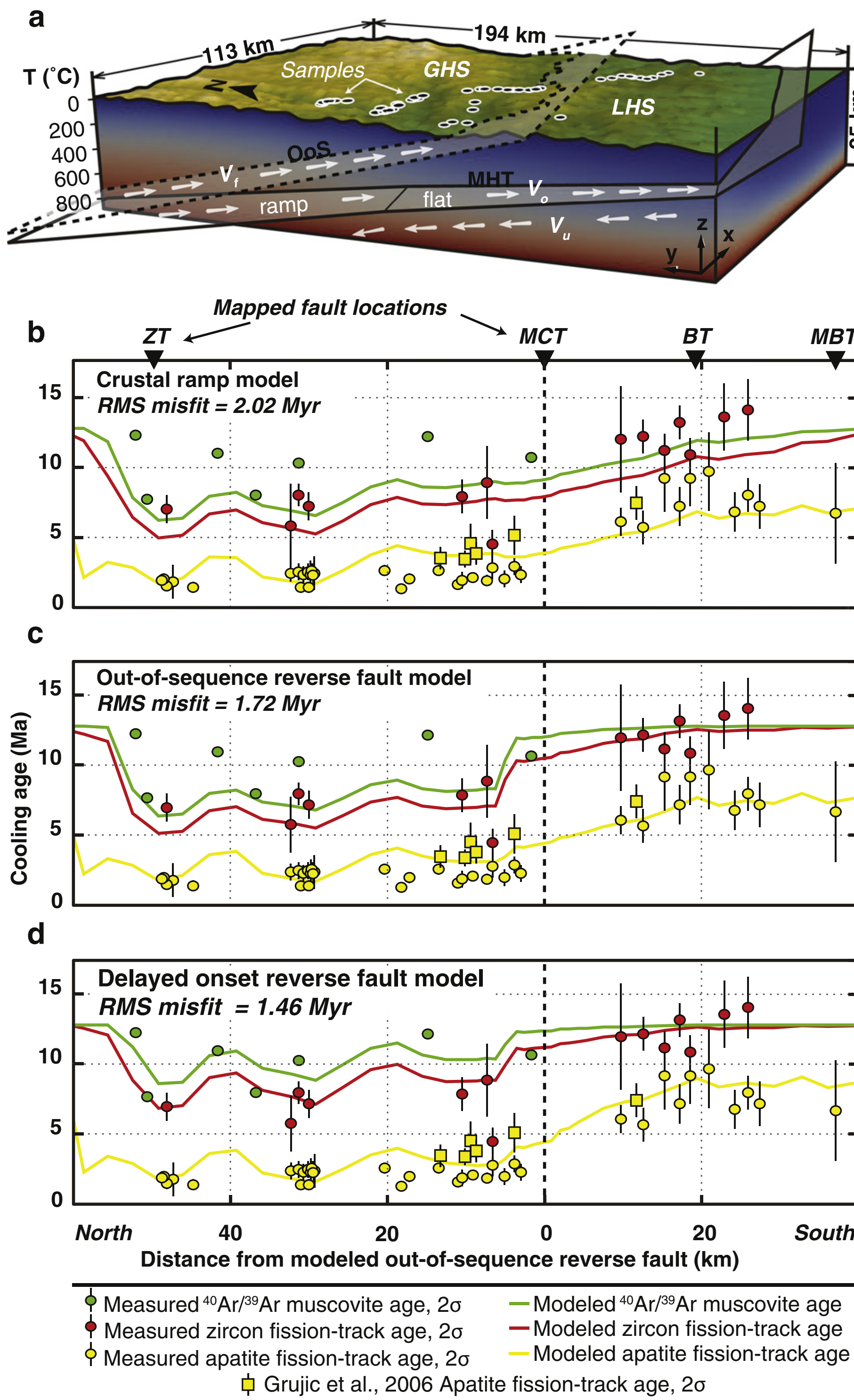

Fig. 4. Schematic model diagram with comparison of observed and model-predicted cooling ages. (a) A 3D schematic block diagram for the thermal–kinematic model, with the surface boundary defined by a digital elevation model of the study area and sample locations plotted on the surface. All models include a crustal-scale flat-ramp (Main Himalayan Thrust) that connects to the Main Frontal Thrust at the surface, and "reverse fault" models include an out-of-sequence reverse fault (OoS), which intersects the surface at the break in cooling ages across the GHS–LHS contact. The geometry and kinematics of these structures are varied as described in the text and Appendix A. Convergence is partitioned into overthrusting (V_o) and underthrusting (V_u) velocities; models that include the out-of-sequence fault further partition V_o between the ramp and the reverse fault (V_f). (b–d) Cooling age data (with 2σ error bars) and model-predicted cooling ages (lines) are plotted vs. distance along the sample transect. Circles show apatite and zircon FT data from this study and muscovite $^{40}Ar/^{39}Ar$ cooling ages from Yin et al. (2010). Squares show apatite FT data from Grujic et al. (2006) located within the model domain for reference. Note that for the $^{40}Ar/^{39}Ar$ data, model predictions are compared to muscovite cooling ages only, and not to ages for neoblastic muscovite or for biotite (which exhibit excess ^{40}Ar) from Yin et al. (2010). The preferred "ramp" model cooling age predictions (lines) are shown in (b), the preferred "reverse fault" model in (c), and the preferred MFT with delayed-onset OoS model in (d). See text and Appendix A for details of the preferred models.

link–lead to rapid, persistent exhumation and deformation. However, our results and the mapping and geochronologic data of Yin et al. (2010) suggest that deformation was not continuous at the orogenic front since the monsoon was established, arguing against not only a spatial but also a temporal correlation of climate-driven erosion patterns and exhumation.

6. Conclusions

Spatial and temporal correlations between high precipitation and rapid long-term erosion and deformation have been documented in several mountain ranges (e.g., Berger et al., 2008; Hodges et al., 2004; Norton and Schlunegger, 2011; Reiners et al., 2003; Thiede et al., 2005), but in the Eastern Himalaya, clear evidence for rapid exhumation deep in the rain shadow of the Shillong Plateau argues against a causal link between the pattern of orographic precipitation and long-term erosion and deformation. Numerical models predict that such links should be strongest in tectonically active settings (e.g., Beaumont et al., 2001; Koons, 1989; Willett, 1999). Yet despite active convergence and a dramatic precipitation gradient that has persisted for millions of years (Biswas et al., 2007; Grujic et al., 2006), long-term erosion in the Eastern Himalaya appears to reflect patterns of rock uplift dictated by fault kinematics. These observations suggest that in this tectonically active setting characterized by steep topography and intense storms, erosion patterns do not mirror precipitation gradients or drive deformation on million-year timescales, but are themselves controlled by tectonic boundary conditions. These findings highlight both the need to better understand how erosive processes scale with precipitation amount and intensity in such settings, and the disconnect between the predictions of geodynamic models and the relationships between climatic gradients as characterized by modern precipitation data and tectonics at the regional scale.

Acknowledgments

This work was supported by funding from a U.S. National Science Foundation grant to K.W.H. (EAR-0955309) and from the Department of Science & Technology, Government of India to R.C.P. (IR/S4/ESF-15/2009). The authors thank Frederic Herman, David Montgomery, and Noah Finnegan for discussions and Harvey Greenberg for GIS assistance. Informal reviews by Djorje Grujic and Juliet Crider and formal reviews by Alex Webb and an anonymous reviewer improved the paper. The authors thank Editor-in-Chief An Yin for encouraging this submission.

Appendix A. Supplementary data and methods

Supplementary data to this article can be found online at http://dx.doi.org/10.1016/j.tecto.2012.09.022.

References

An, Z., Kutzbach, J.E., Prell, W., Porter, S.C., 2001. Evolution of Asian monsoons and phased uplift of the Himalaya–Tibetan plateau since Late Miocene times. Nature 411, 62–66.

Armijo, R., Tapponnier, P., Mercier, J.L., Han, T.-L., 1986. Quaternary extension in southern Tibet: field observations and tectonic implications. Journal of Geophysical Research 91, 13,803–13,872 http://dx.doi.org/10.1029/JB091iB14p13803.

Banerjee, P., Burgmann, R., Nagarajan, B., Apel, E., 2008. Intraplate deformation of the Indian subcontinent. Geophysical Research Letters 35, L18301 http://dx.doi.org/10.1029/2008GL035468.

Beaumont, C., Fullsack, P., Hamilton, J.C., 1992. Erosional control of active compressional orogens. In: McClay, K.R. (Ed.), Thrust Tectonics. Chapman and Hall, New York, pp. 19–31.

Beaumont, C., Jamieson, R.A., Nguyen, M.H., Lee, B., 2001. Himalayan tectonics explained by extrusion of a low-viscosity crustal channel coupled to focused surface denudation. Nature 414, 738–742.

Berger, A.L., Spotila, J.A., Chapman, J.B., Pavlis, T.L., Enkelmann, E., Ruppert, N.A., Buscher, J.T., 2008. Architecture, kinematics, and exhumation of a convergent orogenic wedge: a thermochronological investigation of tectonic–climatic interactions within the central St. Elias orogen, Alaska. Earth and Planetary Science Letters 270, 13–24.

Biswas, S., Coutand, I., Grujic, D., Hager, C., Stockli, D., Grasemann, B., 2007. Exhumation and uplift of the Shillong Plateau and its influence on the Eastern Himalayas: new constraints from apatite and zircon (U–Th–(Sm))/He and apatite fission track analysis. Tectonics 26, TC002125.

Bookhagen, B., Burbank, D.W., 2006. Topography, relief and TRMM-derived rainfall variations along the Himalaya. Geophysical Research Letters 33, L08405 http://dx.doi.org/10.1029/2006GL026037.

Bookhagen, B., Burbank, D.W., 2010. Toward a complete Himalayan hydrological budget: spatiotemporal distribution of snowmelt and rainfall and their impact on river discharge. Journal of Geophysical Research 115, F03019 http://dx.doi.org/10.1029/2009JF001426.

Bookhagen, B., Thiede, R.C., Strecker, M., 2005a. Abnormal monsoon years and their control on erosion and sediment flux in the high, arid northwest Himalaya. Earth and Planetary Science Letters 231, 131–146.

Bookhagen, B., Thiede, R.C., Strecker, M., 2005b. Late Quaternary intensified monsoon phases control landscape evolution in the northwest Himalaya. Geology 33, 149–152.

Braun, J., 2003. Pecube: a new finite element code to solve the heat transport equation in three dimensions in the Earth's crust including the effects of a time-varying, finite amplitude surface topography. Computers & Geosciences 29, 787–794 http://dx.doi.org/10.1016/S0098-3004(03)00052-9.

Braun, J., van der Beek, P., Batt, G., 2006. Quantitative Thermochronology: Numerical Methods for the Interpretation of Thermochronological Data. Cambridge University Press, New York http://dx.doi.org/10.1017/CBO9780511616433 . (258 pp.).

Burbank, D.W., Leland, J., Fielding, E., Anderson, R.S., Brozovic, N., Reid, M.R., Duncan, C., 1996. Bedrock incision, rock uplift and threshold hillslopes in the northwestern Himalayas. Nature 379, 505–510.

Burbank, D.W., Blythe, A.E., Putkonen, J.L., Pratt-Situala, B., Gabet, E.J., Oskin, M.E., Barros, A.P., Ohja, T.P., 2003. Decoupling of erosion and precipitation in the Himalaya. Nature 426, 652–655.

Champagnac, J.-D., van der Beek, P., Diraison, G., Dauphin, S., 2008. Flexural isostatic response of the Alps to increased Quaternary erosion recorded by foreland basin remnants, SE France. Terra Nova 20 (3), 213–220.

Clark, M.K., Bilham, R., 2008. Miocene rise of the Shillong Plateau and the beginning of the end for the Eastern Himalaya. Earth and Planetary Science Letters 269, 337–351 http://dx.doi.org/10.1016/j.epsl.2008.01.045.

Clift, P.D., Hodges, K.V., Heslop, D., Hannigan, R., Van Long, H., Calves, G., 2008. Correlation of Himalayan exhumation rates and Asian monsoon intensity. Nature Geoscience 1, 875–880 http://dx.doi.org/10.1038/ngeo351.

Dahlen, F.A., Suppe, J., 1988. Mechanics, growth, and erosion of mountain belts. In: Clark, S.P., et al. (Ed.), Processes in Continental Lithospheric Deformation: Geol. Soc. Am. Spec. Pap., 218, pp. 161–178.

Das Gupta, A.B., Biswas, A.K., 2000. Geology of Assam. Geol. Soc. India. (169 pp.).

Dettman, D.L., Kohn, M.J., Quade, J., Ryerson, F.J., Ojha, T.P., Hamidullah, S., 2001. Seasonal stable isotope evidence for a strong Asian monsoon throughout the last 10.7 Ma. Geology 29, 31–34.

Dettman, D.L., Fang, X., Garzione, C.N., Li, J., 2003. Uplift-driven climate change at 12 Ma: a long $\delta^{18}O$ record from the NE margin of the Tibetan plateau. Earth and Planetary Science Letters 214, 267–277.

DiBiase, R.A., Whipple, K.X., 2011. The influence of erosion thresholds and runoff variability on the relationships among topography, climate, and erosion rate. Journal of Geophysical Research 116, F04036 http://dx.doi.org/10.1029/2011JF002095.

Dunlap, W.J., Hirth, G., Teyssier, C., 1997. Thermomechanical evolution of a ductile duplex. Tectonics 16, 983–1000 http://dx.doi.org/10.1029/97TC00614.

Foster, D.A., Gleadow, A.J., Reynolds, S.J., Fitzgerald, P.G., 1993. Denudation of metamorphic core complexes and the reconstruction of the transition zone, west central Arizona: constraints from apatite fission track thermochronology. Journal of Geophysical Research 98 (B2), 2167–2185.

Gabet, E.J., Burbank, D.W., Pratt-Sitaula, B., Putkonen, J., Bookhagen, B., 2008. Modern erosion rates in the high Himalayas of Nepal. Earth and Planetary Science Letters 267, 482–494 http://dx.doi.org/10.1016/j.epsl.2007.11.059.

Gansser, A., 1983. Geology of the Bhutan Himalaya. Birkhauser Verlag, Stuttgart.

Grujic, D., Hollister, L., Parrish, R., 2002. Himalayan metamorphic sequence as an orogenic channel: insight from Bhutan. Earth and Planetary Science Letters 198, 177–191.

Grujic, D., Coutand, I., Bookhagen, B., Bonnet, S., Blythe, A., Duncan, C., 2006. Climatic forcing of erosion, landscape, and tectonics in the Bhutan Himalayas. Geology 34, 801–804.

Guo, Z.T., Ruddiman, W.F., Hao, Q.Z., Wu, H.B., Qiao, Y.S., Zhu, R.X., Peng, S.Z., Wei, J.J., Yan, B.Y., Liu, T.S., 2002. Onset of Asian desertification by 22 Myr ago inferred from loess deposits in China. Nature 416, 159–163.

Harrison, T.M., Celerier, J., Ailkman, A.B., Hermann, J., Heizler, M., 2009. Diffusion of ^{40}Ar in muscovite. Geochimica et Cosmochimica Acta 73, 1039–1051 http://dx.doi.org/10.1016/j.gca.2008.09.038.

Herman, F., Copeland, P., Avouac, J.P., Bollinger, L., Mahéo, G., Le Fort, P., Rai, S., Foster, D., Pêcher, A., Stüwe, K., Henry, P., 2010. Exhumation, crustal deformation, and thermal structure of the Nepal Himalaya derived from the inversion of thermochronological and thermobarometric data and modeling of the topography. Journal of Geophysical Research 115, B06407 http://dx.doi.org/10.1029/2008JB006126.

Hilley, G.E., Coutand, I., 2010. Links between topography, erosion, rheological heterogeneity, and deformation in contractional settings: insights from the central Andes. Tectonophysics 495, 78–92.

Hodges, K.V., 2000. Tectonics of the Himalaya and southern Tibet from two perspectives. Geological Society of America Bulletin 112 (3), 324–350.

Hodges, K.V., Wobus, C., Ruhl, K., Schildgen, T., Whipple, K., 2004. Quaternary deformation, river steepening and heavy precipitation at the front of Higher Himalayan ranges. Earth and Planetary Science Letters 220, 379–389.

Huntington, K.W., Hodges, K.V., 2006. A comparative study of detrital mineral and bedrock age-elevation methods for estimating erosion rates. Journal of Geophysical Research 111, F03011 http://dx.doi.org/10.1029/2005JF000454.

Huntington, K.W., Blythe, A.E., Hodges, K.V., 2006. Climate change and Late Pliocene acceleration of erosion in the Himalaya. Earth and Planetary Science Letters 252, 107–118.

Iaffaldano, G., Husson, L., Bunge, H.-P., 2011. Monsoon speeds up Indian plate motion. Earth and Planetary Science Letters 304, 503–510.

Jackson, M., Bilham, R., 1994. Constraints on Himalayan deformation inferred from vertical velocity fields in Nepal and Tibet. Journal of Geophysical Research 99, 13897–13912.

Ketcham, R.A., Carter, A., Donelick, R.A., Barbarand, J., Hurford, A.J., 2007. Improved modeling of fission-track annealing in apatite. American Mineralogist 92, 799–810 http://dx.doi.org/10.2138/am.2007.2281.

Koons, P.O., 1989. The topographic evolution of collisional mountain belts: a numerical look at the Southern Alps, New Zealand. American Journal of Science 289, 1041–1069.

Koons, P.O., Zeitler, P.K., Chamberlain, C., Craw, D., Meltzer, A.S., 2002. Mechanical links between erosion and metamorphism in Nanga Parbat, Pakistan Himalaya. American Journal of Science 302, 749–773.

Koons, P.O., Norris, R.J., Craw, D., Cooper, A.F., 2003. Influence of exhumation of the structural evolution of transpressional plate boundaries: an example from the Southern Alps, New Zealand. Geology 31, 3–6 http://dx.doi.org/10.1130/0091-7613(2003) 031<0003:IOEOTS>2.0.CO;2.

Koppes, M.N., Montgomery, D.R., 2009. The relative efficacy of fluvial and glacial erosion over modern to orogenic timescales. Nature Geoscience 2, 644–647 http://dx.doi.org/10.1038/ngeo616.

Lague, D., Hovius, N., Davy, P., 2005. Discharge, discharge variability, and the bedrock channel profile. Journal of Geophysical Research 110 (F4) http://dx.doi.org/10.1029/2004JF000259.

LeFort, P., 1975. Himalayas: the collided range. Present knowledge of the continental arc. American Journal of Science 275-A, 1–44.

Long, S., McQuarrie, N., Tobgay, T., Rose, C., Gehrels, G., Grujic, D., 2011. Tectonostratigraphy of the lesser Himalaya of Bhutan: implications for the along-strike stratigraphic continuity of the northern Indian margin. Geological Society of America Bulletin http://dx.doi.org/10.1130/B30202.1.

McQuarrie, N., Robinson, D., Long, S., Tobgay, T., Grujic, D., Gehrels, G., Ducea, M., 2008. Preliminary stratigraphic and structural architecture of Bhutan: implications for the along strike architecture of the Himalayan system. Earth and Planetary Science Letters 272, 105–117 http://dx.doi.org/10.1016/j.epsl.2008.04.030.

Molnar, P., 2001. Climate change, flooding in arid environments, and erosion rates. Geology 29 (12), 1071–1074 http://dx.doi.org/10.1130/0091-7613(2001) 029<1071:CCFIAE>2.0.CO;2.

Molnar, P., England, P., Martinod, J., 1993. Mantle dynamics, uplift of the Tibetan Plateau, and the Indian monsoon. Reviews of Geophysics 31, 357–396.

Molnar, P., Anderson, R.S., Anderson, S.P., 2007. Tectonics, fracturing of rock, and erosion. Journal of Geophysical Research, Earth Surface 112, F03014 http://dx.doi.org/10.1029/2005JF000433.

Norton, K., Schlunegger, F., 2011. Migrating deformation in the Central Andes from enhanced orographic rainfall. Nature Communications 2 http://dx.doi.org/10.1038/ncomms1590.

Patel, R.C., Adlakha, V., Lal, N., Singh, P., Kumar, Y., 2011. Spatiotemporal variation in exhumation of the crystallines in the NW-Himalaya, India: constraints from fission track dating analysis. Tectonophysics 504, 1–13.

Reiners, P.W., Ehlers, T.A., Mitchell, S.G., Montgomery, D.R., 2003. Coupled spatial variation in precipitation and long-term erosion rates across the Washington Cascades. Nature 426, 645–647.

Robert, X., van der Beek, P., Braun, J., Perry, C., Mugnier, J.L., Perry, C., Dubille, M., 2009. Assessing Quaternary reactivation of the Main Central Thrust zone (central Nepal Himalaya): new thermochronologic data and numerical modelling. Geology 37, 731–734.

Robert, X., van der Beek, P., Braun, J., Perry, C., Mugnier, J.L., 2011. Control of detachment geometry on lateral variations in exhumation rates in the Himalaya: insights from low-temperature thermochronology and numerical modeling. Journal of Geophysical Research 116, B05202 http://dx.doi.org/10.1029/2010JB007893.

Roe, G.H., Brandon, M.T., 2011. Critical form and feedbacks in mountain-belt dynamics: role of rheology as a tectonic governor. Journal of Geophysical Research 116, B02101 http://dx.doi.org/10.1029/2009JB006571.

Styron, R.H., Taylor, M.H., Murphy, M.A., 2011. Oblique convergence, arc-parallel extension, and the role of strike-slip faulting in the High Himalaya. Geosphere 7, 582–596 http://dx.doi.org/10.1130/GES00606.1.

Sun, X., Wang, P., 2005. How old is the Asian monsoon system? Palaeobotanical records from China. Palaeogeography, Palaeoclimatology, Palaeoecology 222, 181–222.

Tagami, T., Shimada, C., 1996. Natural long-term annealing of the zircon fission track system around a granitic pluton. Journal of Geophysical Research 101, 8245–8255 http://dx.doi.org/10.1029/95JB02885.

Taylor, M., Yin, A., Ryerson, F., Kapp, P., Ding, L., 2003. Conjugate strike-slip fault accommodates coeval north-south shortening and east-west extension along the Bangong-Nujiang suture zone in central Tibet. Tectonics 22 http://dx.doi.org/10.1029/2002TC001361.

Thiede, R.C., Arrowsmith, J.R., Bookhagan, B., Mcwilliams, M.O., Sobel, E.R., Strecker, M.R., 2005. From tectonically to erosionally controlled development of the Himalayan orogen. Geology 33, 689–692.

Thiede, R.C., Ehlers, T.A., Bookhagan, B., Strecker, M.R., 2009. Erosional variability along NW Himalaya. Journal of Geophysical Research http://dx.doi.org/10.1029/2008JF001010.

Tobgay, T., McQuarrie, N., Long, S., Kohn, M.J., Corrie, S.L., 2012. The age and rate of displacement along the Main Central Thrust in the western Bhutan Himalaya. Earth and Planetary Science Letters 319–320, 146–158.

Tucker, G.E., Bras, R.L., 2000. A stochastic approach to modeling the role of rainfall variability in drainage basin evolution. Water Resources Research 36, 1953–1964 http://dx.doi.org/10.1029/2000WR900065.

Tucker, G.E., Slingerland, R., 1997. Drainage basin response to climate change. Water Resources Research 33, 2031–2047.

Vernon, A.J., van der Beek, P.A., Sinclair, H.D., 2009. Spatial correlation between long-term exhumation rates and present-day forcing parameters in the western European Alps. Geology 37, 859–862 http://dx.doi.org/10.1130/G25740A.1.

Whipple, K.X., 2009. The influence of climate on the tectonic evolution of mountain belts. Nature Geoscience 2, 97–104.

Willett, S.D., 1999. Orogeny and orography: the effects of erosion on the structure of mountain belts. Journal of Geophysical Research 104, 28957–28981.

Willett, S.D., Beaumont, C., Fullsack, P., 1993. Mechanical model for the tectonics of doubly vergent compressional orogens. Geology 21, 371–374.

Wobus, C.W., Hodges, K.V., Whipple, K.X., 2003. Has focused denudation sustained active thrusting at the Himalayan topographic front? Geology 31, 861–864 http://dx.doi.org/10.1130/G19730.1.

Wobus, C.W., Heimsath, A., Whipple, K., Hodges, K., 2005. Active out-of-sequence thrust faulting in the central Nepalese Himalaya. Nature 434, 1008–1011.

Yin, A., 2000. Mode of Cenozoic east–west extension in Tibet suggesting a common origin of rifts in Asia during the Indo-Asian collision. Journal of Geophysical Research 105, 21745–21759 http://dx.doi.org/10.1029/2000JB900168.

Yin, A., 2006. Cenozoic tectonic evolution of the Himalayan orogen as constrained by along-strike variation of structural geometry, exhumation history, and foreland sedimentation. Earth-Science Reviews 76, 1–131.

Yin, A., Dubey, C.S., Kelty, T.K., Gehrels, G.E., Chou, C.Y., Grove, M., Lovera, O., 2006. Structural evolution of the Arunachal Himalaya and implications for asymmetric development of the Himalayan orogen. Current Science 90 (2), 195–206.

Yin, A., Dubey, C.S., Kelty, T.K., Webb, A.A.G., Harrison, T.M., Chou, C.Y., Célérier, J., 2010. Geologic correlation of the Himalayan orogen and Indian craton: part 2. Structural geology, geochronology, and tectonic evolution of the Eastern Himalaya. Geological Society of America Bulletin 122, 360–395 http://dx.doi.org/10.1130/B26461.1.